Bioorganic & Medicinal Chemistry Letters 30 (2020) 127405

Contents lists available at ScienceDirect

Bioorganic & Medicinal Chemistry Letters

journal homepage: www.elsevier.com/locate/bmcl

Structure-guided optimization of a novel class of ASK1 inhibitors with increased sp^3 character and an exquisite selectivity profile

Simone V. Bigi-Botterill[a,*], Anthony Ivetac[b], Erica L. Bradshaw[c], Derek Cole[a], Douglas R. Dougan[d], Jacques Ermolieff[a], Petro Halkowycz[a], Ben Johnson[e], Christopher McBride[f], Jason Pickens[a], Mark Sabat[a], Steven Swann[g]

[a] Medicinal Chemistry & In Vitro Pharmacology, Gastroenterology Drug Discovery Unit, Takeda Research in California, 9625 Towne Centre Drive, San Diego, CA 92121, United States
[b] Mirati Therapeutics, 9393 Towne Centre Drive #200, San Diego, CA 92121, United States
[c] Quantitative Translational Sciences, Takeda Research in California, 9625 Towne Centre Drive, San Diego, CA 92121, United States
[d] Structural Biology & Biophysics, Gastroenterology Drug Discovery Unit, Takeda Research in California, 9625 Towne Centre Drive, San Diego, CA 92121, United States
[e] Medicinal Chemistry, Neuroscience Drug Discovery Unit, Takeda Research in California, 9625 Towne Centre Drive, San Diego, CA 92121, United States
[f] 858 Therapeutics, 4757 Nexus Center Drive #150, San Diego, CA 92121, United States
[g] Chemistry & Design, Silicon Therapeutics, 451 D Street #205, Boston, MA 02210, United States

ARTICLE INFO

Keywords:
Mitogen-Activated Protein Kinase Kinase Kinase (MAP3K)
Apoptosis Signal-Regulating Kinase-1 (ASK1)
Structure-Based Drug Design (SBDD)
Cardiac injury
Kinome selectivity

ABSTRACT

Apoptosis Signal-Regulating Kinase-1 (ASK1) is a known member of the Mitogen-Activated Protein Kinase Kinase Kinase (MAP3K) family and upon stimulation will activate the p38- and JNK-pathways leading to cardiac apoptosis, fibrosis, and hypertrophy. Using Structure-Based Drug Design (SBDD) in parallel with deconstruction of a published compound, a novel series of ASK1 inhibitors was optimized, which incorporated a saturated heterocycle proximal to the hinge-binding motif. This yielded a unique chemical series with excellent selectivity across the broader kinome, and desirable drug-like properties. The lead compound (**10**) is highly soluble and permeable, and exhibits a cellular EC_{50} = 24 nM and K_d < 1 nM. Of the 350 kinases tested, **10** has an $IC_{50} \leq 500$ nM for only eight of them. This paper will describe the design hypotheses behind this series, key data points during the optimization phase, as well as a possible structural rationale for the kinome selectivity. Based on crystallographic data, the presence of an aliphatic cycle adjacent to the hinge-binder in the active site of the protein kinase showed up in < 1% of the > 5000 structures in the Protein Data Bank, potentially conferring the selectivity seen in this series.

Kinases are amongst the most extensively studied protein families based on the vast number of structures currently available in the Protein Data Bank (PDB) and continue to be attractive targets in a variety of diseases. In a 2016 analysis of FDA-approved small molecule kinase inhibitors, Wu et al. determined that of the 28 approved drugs, 25% were considered “promiscuous” wherein they exhibited less than 20-fold selectivity over more than ten off-targets.[1,2] Considering this and the high structural similarity between the ATP-binding pockets of different kinases, selectivity can be a challenge when optimizing kinase inhibitors. For chronic, non-oncology indications, a need for highly selective kinase inhibitors still exists.

The Mitogen-Activated Protein Kinase Kinase Kinase (MAP3K) family mediates a wide array of cellular signaling events and inflammatory responses. Within this pathway, Apoptosis Signal-Regulating Kinase-1 (ASK1 or MAP3K5) is activated by various extracellular stimuli including cytokines, endoplasmic reticulum (ER) stressors, and reactive oxygen species (ROS). In turn, ASK1 will phosphorylate its downstream MAP Kinase Kinase (MKK) effectors, MKK3/6 and MKK4/7, leading to activation of the p38- and JNK-pathways, respectively (Fig. 1).[3,4]

Although ASK1 signaling has primarily been of interest in the field of immunology, there is evidence supporting its role in several other therapeutic areas.[5] The function of ASK1 in the pathophysiology of ischemia and heart failure has been demonstrated where its overexpression can lead to cardiac apoptosis, fibrosis, and hypertrophy.[6,7] More recently, the pathogeneses of certain cardiovascular diseases, non-alcoholic fatty liver disease (NAFLD), and non-alcoholic steatohepatitis (NASH) have been linked through similar mechanisms

* Corresponding author.
E-mail address: simone.bigi@takeda.com (S.V. Bigi-Botterill).

https://doi.org/10.1016/j.bmcl.2020.127405
Received 19 May 2020; Received in revised form 6 July 2020; Accepted 7 July 2020
Available online 12 July 2020
0960-894X/ Published by Elsevier Ltd. This is an open access article under the CC BY-NC-ND license (http://creativecommons.org/licenses/BY-NC-ND/4.0/).

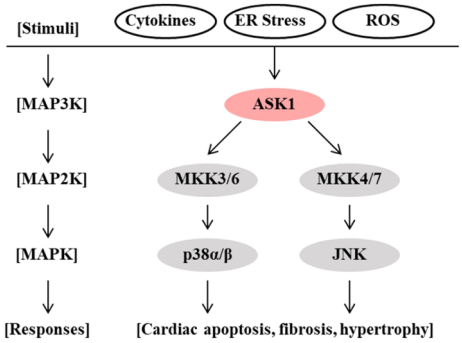

Fig. 1. MAPKKK (MAP3K) signaling pathway. Inhibition of ASK1 could attenuate cardiac inflammation.

delineating ASK1 as a suitable target for therapeutic intervention.[8] There has also been a renewed interest in targeting ASK1 for cancer indications, specifically targeting cancer cells with multidrug resistance (MDR) from over-expression of efflux transporters.[9]

To help validate the cardioprotective role of inhibiting ASK1, our initial goal was to generate a potent and selective small-molecule inhibitor to profile in key *in vivo* experiments. Several parallel efforts in pursuit of novel, potent, and orally bioavailable ASK1 inhibitors to interrogate therapeutic hypotheses around ASK1 biology have been disclosed by Takeda, including the discovery of a series containing an isoindolinone core (**1**, Fig. 2A). A co-crystal structure of **1** bound in the ASK1 ATP-binding site confirmed the hydrogen bond to the hinge of the kinase through the carbonyl of the isoindolinone and the valine residue (Val757) backbone N−H. The planarity of the hinge-binding motif is maintained by the adjacent pyridine, while also providing a flat trajectory for the isopropyl-triazole to sit and hydrogen bond to the conserved catalytic lysine (Lys709). The isopropyl group fills a small hydrophobic pocket.[10] To-date, one of the most advanced clinical stage ASK1-targeting compounds is Selonsertib (**2**, Fig. 2B), which in February 2019 failed to meet its primary endpoint in a Phase III clinical study in patients with NASH. However, **2** demonstrates efficacy against cancer cells with overexpression of ATP-binding cassette (ABC) transporters: ABC1 and ABCG2.[9,11,12]

Also efficacious in a mouse ischemia/reperfusion model, **2** led to a dose-dependent reduction in infarct size (31% for 10 mg/kg ($P < 0.001$) and 60% for 30 mg/kg ($P < 0.001$)) and preservation of left ventricular systolic function.[13,14] Although this compound lacked a crystal structure and its profile was not suitable for our purposes, it guided an integrated lead generation strategy around public/in-house crystal structures and structure-based drug design (SBDD). Despite the lack of structural data for **2**, hypotheses regarding its potential binding mode supported an integrated approach to novel lead discovery. Deconstruction of **2** illustrated the different contributions of the scaffold constituents to its overall potency and is shown in Fig. 2B. Pairing this information with an overlay of the crystal structure of **1** and a model of **2** highlighted the varying importance on activity of two specific interactions with ASK1: the glycine in the solvent-exposed region (Gly759) and Lys709. When the cyclopropyl imidazole was removed, potency decreased by 18-fold, **3**. From modeling, it seemed possible that the cyclopropyl imidazole was π-stacking over the N−H of Gly759 — an interaction Takeda previously published in crystal structures from two different ASK1 inhibitor series.[15,16] Removal of the isopropyl-triazole (**4**) resulted in a 2000-fold loss in potency to an IC_{50} of 6.0 μM, which was accompanied by an expected decrease in the ligand efficiency ($LE = -\Delta G/HAC \sim -RT\ln(IC_{50})/HAC$; the free energy of binding divided by heavy atom count) and the lipophilic ligand efficiency ($LLE = pIC_{50}$-cLogD, where cLogD is the calculated logarithm of the octanol/water partition coefficient measured at pH of 7.4.[17,18] Essentially, removing the hydrogen bond to Lys709 removes most ASK1 activity.

The severe drop in potency resulting from removal of the isopropyl triazole of **4** focused optimization toward other regions of the molecule. The co-planar, ring system served as an attractive starting point because of the ability to manipulate and mimic this type of shape—or lack thereof. Numerous strategies were used to imitate this conformation

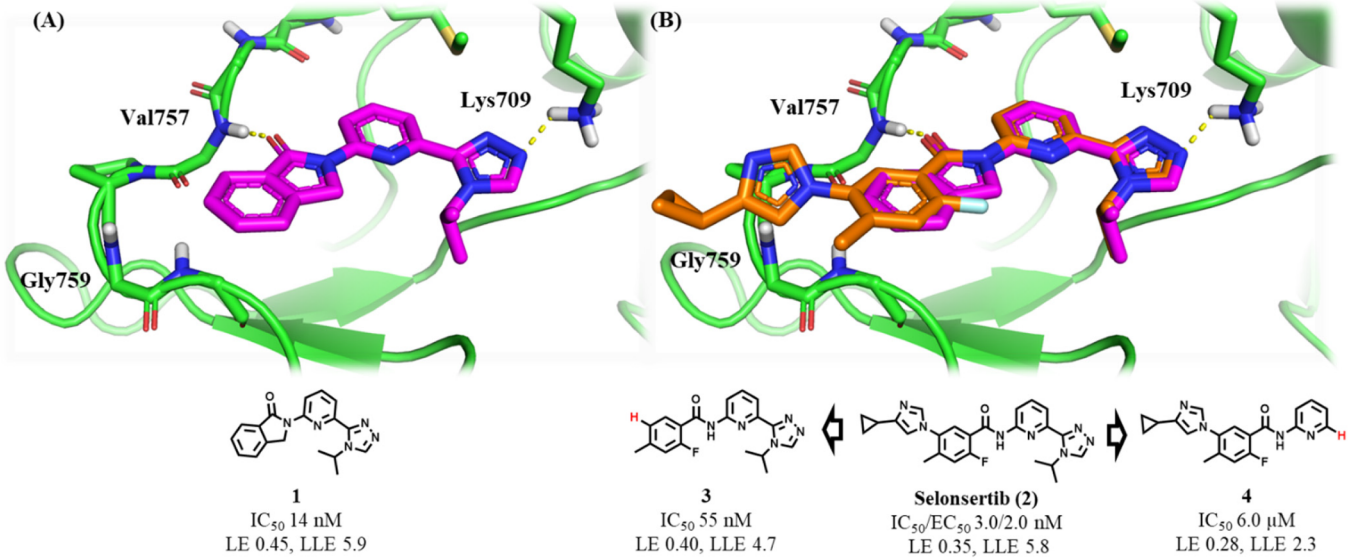

Fig. 2. (A) A crystal structure of **1** bound in the ASK1 ATP site to a resolution of 2.95 Å (PDB: 5UP3). Enzymatic/cellular potency is shown with ligand efficiency (LE) and lipophilic ligand efficiency (LLE). (B) Deconstruction around Gilead Sciences Phase III inhibitor, **Selonsertib** or **2**. A model of **2** (in orange) was overlaid with the crystal structure of **1** (magenta). The figures were generated using Pymol®.

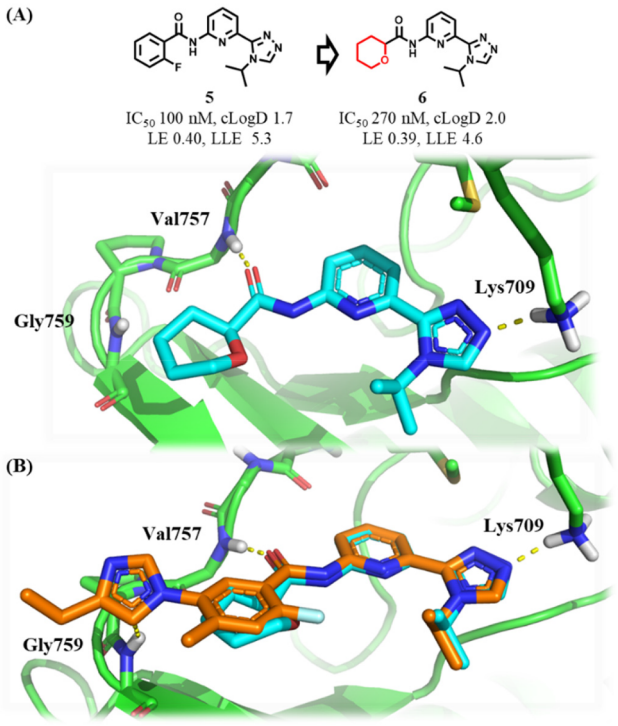

Fig. 3. (A) Crystal structure of **6** bound in the ASK1 ATP site to a resolution of 2.65 Å (PDB: 6XIH). (B) An overlay of the ASK1 crystal structure of **6** (in turquoise) and a model of **2** (in orange). The figures were generated using Pymol®.

while modulating physical properties through ring modifications and substitutions, specifically retaining the stabilized hinge-binding benzamide while providing a vector towards Gly759.

An interesting compound that emerged from this exercise incorporated a non-aromatic ether group adjacent to the hinge amide (**6**, Fig. 3A). This substitution showed only a moderate decrease in potency relative to a comparator, **5**. A co-crystal structure of this compound bound to ASK1 was acquired and confirmed the anticipated binding mode (Fig. 3A). An overlay of the crystal structure of **6** with the model of **2** showed the inhibitors had a high degree of overlap, with the tetrahydropyran sitting in similar chemical space to the phenyl group, with a clear vector to grow towards Gly759 (Fig. 3B).

Compound **6** showed improved selectivity compared to **1** when tested in a kinase selectivity mini-panel (Table 1), which supported

Table 1
Selectivity of **6** versus **1** against other MAP3K kinases in a binding assay at a top concentration of 10 μM. Potencies are listed as pIC_{50} values.

Kinase	6	1
ASK1	6.6	7.9
PRKKA1	< 4.7	6.7
p38	< 4.7	< 4.7
EGFR	< 4.7	< 4.7
HER4	< 4.7	< 4.7
MER	< 4.7	6.2
RET	< 4.7	7.2
ROCK1	< 4.7	6.0
ITK	< 4.7	5.9
ERBB4	< 4.7	< 4.7
EPHA3	< 4.7	< 4.7
GSK3	6.2	7.4
CDK2	5.5	7.2

further optimization of this scaffold.

Summarized in Fig. 4A, replacement of the tetrahydropyran with a morpholine ring (**7**), although less potent than **6**, had a higher LLE value representing a more compelling starting point with a lower cLogD. Modeling of **7** alongside **2** suggested extending from the morpholine nitrogen could provide a vector to engage Gly759, thus providing an opportunity to increase potency while also modulating the basicity of the amine in an area of the active site where polarity is not typically tolerated. The addition of the phenyl group provided a modest increase in enzymatic potency to 130 nM (**8**). By adding a nitrogen to the ring, clogD was lowered while the potency increased by 4-fold (**9**), resulting in an almost two log unit increase in LLE. The addition of a cyclopropyl further increased potency and, by isolating the more active enantiomer, a novel lead compound (**10**) was identified with a cellular EC_{50} = 24 nM and a K_d < 1 nM. Based on the model of **10** bound in the ASK1 active site (Fig. 4B), and its cellular activity, it was concluded the pyridine was stacking over Gly759.

The physiochemical properties and a subset of ADME (absorption, distribution, metabolism, and elimination) properties of **10** are summarized in Fig. 4C. Overall, the physiochemical properties of this molecule are favorable, including three aryl rings and cLogD 2.1. Pharmacokinetic (PK) studies were performed in rats where the inhibitor was well absorbed; however, its high clearance led to low oral bioavailability (%F, see Supplementary Data for full ADME and PK profiles). Selectivity was investigated across an Invitrogen™ panel of 350 kinases (representing > 50% of the predicted human kinome). Compound **10** showed exquisite selectivity where only eight kinases were inhibited with an $IC_{50} \leq 500$ nM (< 20-fold selective). Full dose-response curves at a top concentration of 30 μM were generated for those eight kinases, and their IC_{50} data is shown boxed in Fig. 5. This data highlights that **10** is a highly selective inhibitor of ASK1.

To help explain the impressive kinome selectivity of **10**, we examined the residues at positions lining the modeled morpholine location. Of interest was the "GGSL" sequence containing the Gly759 residue that, when engaged, appears to enhance ASK1 activity. However, this sequence was not found to be particularly rare within the human kinome. Suggestive of a role for the sp^3-rich morpholine towards target selectivity, we mined all human protein kinase crystal structures reported in the PDB using a 3D search of all bound kinase ligands with a variety of aliphatic 6-membered rings in that region of the ATP pocket (see Supplementary Material).

Our results (Table 2) indicated that aliphatic ring systems are particularly rare in this sub-region annexing the hinge, with the morpholine appearing in < 1% of the 5,490 kinase structures analyzed. By contrast, flat, aromatic, 6-membered rings are significantly more prevalent— with phenyl, for example, occurring in this sub-region in 31.3% of all kinase structures. While this analysis is limited to the small region of chemical and protein space covered by crystal co-complexes, one could speculate that the ASK1 ATP pocket can accommodate both aliphatic and aromatic groups at this location, with an aliphatic group imparting increased selectivity for this target. The structural basis for the selectivity seen in this series could be borne from the conformational dynamics of the ASK1 pocket, which may be able to form the cavity required to accept both flat and globular rings.

In summary, a multi-prong lead generation strategy utilizing deconstruction and SBDD resulted in a novel chemical series with desirable drug-like properties and exquisite selectivity across the broader kinome (Fig. 6). Mining the PDB for saturated, cyclic pharmacophores highlighted how unique a morpholine is in that region of a kinase active site, appearing in < 1% of the 5,490 kinase structures analyzed. The utility of this approach to parameterized searching of chemical space for novel functional groups could be a useful strategy for kinase drug discovery.

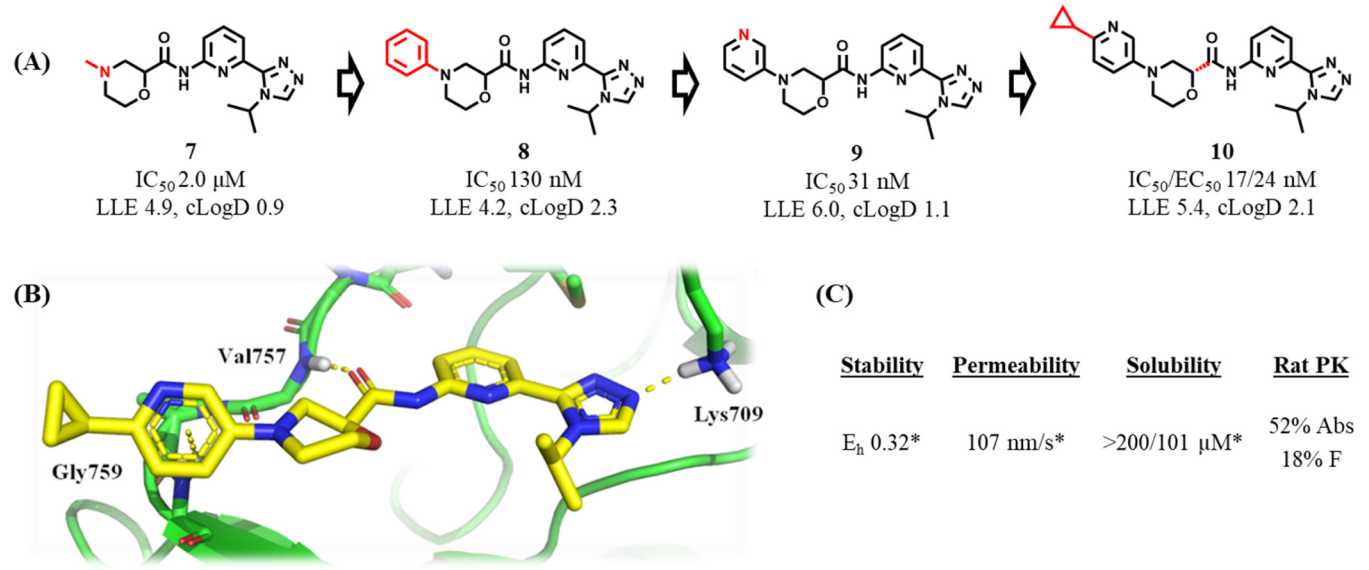

Fig. 4. (A) Optimization to a nanomolar inhibitor. (B) A model of **10** in the ASK1 ATP site was generated using Pymol®. (C) Physiochemical property data, absorption, and bioavailability (%F) for **10** (*data for racemate). Stability in human hepatocytes shown as hepatic extraction ratio (E_h) measured as hepatic clearance/species-specific liver blood flow. Membrane permeability in LLC-PK1-MDR1 cell line shown as the movement from the apical compartment to the basolateral compartment. Kinetic solubility shown as JP1(pH 1.2)/JP2(pH 6.5). Pharmacokinetic studies (PK) in male Sprague-Dawley rats: dosed at 1 $mgkg^{-1}$ IV (n = 2, 20% β-cyclodextrin in 0.05 M methanesulfonic acid, pH 3) and 5 $mgkg^{-1}$ PO (n = 3, 20% β-cyclodextrin in 0.05 M methanesulfonic acid, pH 3).

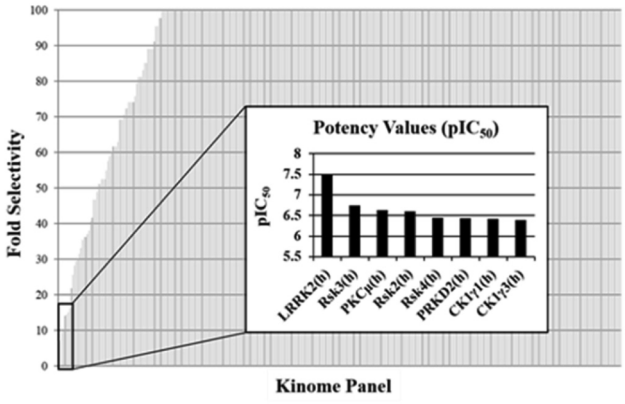

Fig. 5. Selectivity profile of **10** against an Invitrogen™ panel of 350 kinases. The box highlights the eight kinases the inhibitor exhibited < 20-fold selectivity over, with their potencies listed in the chart.

Table 2
Occurrence of various aliphatic versus aromatic rings in the "morpholine pocket" of the human protein kinases in the PDB.

Aliphatic Ring System	Count	0.7%
Tetrahydropyran	1	
Morpholine	7	0.1%
Piperidine	1	
Piperazine	3	
Cyclohexane	25	
Aromatic Ring System	**Count**	**34.6%**
Phenyl	1,717	31.3%
Pyridine	66	
Pyrimidine	116	

Declaration of Competing Interest

The authors declare that they have no known competing financial interests or personal relationships that could have appeared to influence the work reported in this paper.

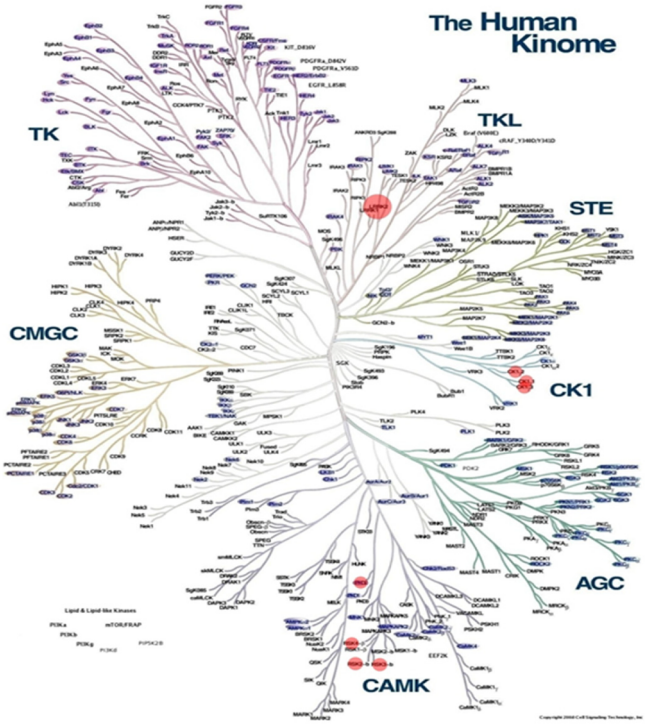

Fig. 6. A kinome dendrogram selectivity plot of **10** highlights the 8/350 kinases with $IC_{50} \leq 500$ nM. The larger the circle that more active against that kinase. Illustration reproduced courtesy of Cell Signaling Technology, Inc. (www.cellsignal.com).

Acknowledgments

We would like to thank Charles E. Grimshaw for his help generating selectivity data. We would also like to thank Steve Woodhead and Tony Gibson for reviewing this manuscript. The staff of the Berkeley Center for Structural Biology is gratefully acknowledged for support of beamline 5.0.3 at the Advanced Light Source. The Advanced Light

Source is supported by the Director, Office of Science, Office of Basic Energy Sciences, of the U.S. Department of Energy under Contract No. DE-AC02-05CH11231. This research was also resourced by the Advanced Photon Source, a U.S. Department of Energy (DOE) Office of Science User Facility operated for the DOE Office of Science by Argonne National Laboratory under Contract No. DE-AC02-06CH11357.

Appendix A. Supplementary data

Included are protocols for (1) synthetic procedures for **10**, including NMR and LC/MS spectra, (2) pharmacokinetic (PK) evaluation, (3) mining the region-of-interest in the ATP-binding site of kinases in the PDB using MOE®.[19] Supplementary data to this article can be found online at https://doi.org/10.1016/j.bmcl.2020.127405.

References

1. Wu P, Nielsen TE, Clausen MH. *Trends Pharmacol Sci.* 2015;36:422–439.
2. Wu P, Nielsen TE, Clausen MH. *Drug Discov Today.* 2016;21:5–10.
3. Ichijo H, Nishida E, Irie K, et al. *Science.* 1997;275:90–94.
4. Nagai H, Noguchi T, Takeda K, Ichijo H. *J Biochem Mol Biol.* 2007;40:1–6.
5. Kawarazaki Y, Ichijo H, Naguro I. *Expert Opin Ther Tar.* 2014;18:651–654.
6. Wang Y, Huang S, Sah VP, et al. *J Biol Chem.* 1998;273:2161–2168.
7. Zarubin T, Han J. *Cell Res.* 2005;15:11–18.
8. Schuster S, Feldstein A. *Nat Rev Gastroenterol Hepatol.* 2017;14:329–330.
9. Ji N, Yang Y, Lei ZN, et al. *Cancer Lett.* 2019;440–441:82–93.
10. Lanier M, Pickens J, Bigi SV, et al. *ACS Med Chem Lett.* 2017;8:316–320.
11. https://clinicaltrials.gov/ct2/show/NCT03053063.
12. https://clinicaltrials.gov/ct2/show/NCT03053050.
13. Toldo S, Breckenridge DG, Mezzaroma E, et al. *Am Heart Assoc.* 2015:1–9.
14. Gilead Sciences, INC (2014). Apoptosis signal-regulating kinase inhibitor. US8742126B2.
15. Terao Y, Suzuki H, Yoshikawa M, et al. *Bioorg Med Chem Lett.* 2012;22:7326–7329.
16. Takeda Pharmaceutical Company LTD (2014). Apoptosis signal-regulating kinase 1 inhibitors. US8921358B2.
17. Hopkins AL, Groom CR, Alex A. *Drug Discov Today.* 2004;9:430–431.
18. Leeson PD, Springthorpe B. *Nat Rev Drug Discov.* 2007;6:881–890.
19. Molecular Operating Environment (MOE), 2019; Chemical Computing Group Inc., 1010 Sherbooke St. West, Suite #910, Montreal, QC, Canada, H3 A 2R7, 2019.